This is the pre-peer reviewed version of the following article: **[J. Reolid; C. Betzler. Ichnofabric logs for the characterization of the organic content in carbonates. Marine and Petroleum Geology. 95, pp. 246 - 254. 2018.]**, which has been published in final form at **[https://doi.org/10.1016/j.marpetgeo.2018.04.019].** This article may be used for non-commercial purposes in accordance with Elsevier Terms and Conditions for Use of Self-Archived Versions

Abstract

This study proposes an approach to visualize ichnological data from cores that allows direct comparison with downhole logs. It provides preliminary but accurate environmental information, especially on the oxygenation and/or the organic matter content at the sea-floor. The method comprises three steps: Step 1) ichnological analysis of the sediments including quantification of bioturbation intensity, identification of the main ichnotaxa and sizes of the burrows, depth of burrowing or tiering, and documentation of cross-cutting relationships; Step 2) ichnofabric definition following a series of criteria including the bioturbation index, the ichnoassemblage, and the sediment type; and Step 3) the organization of the ichnofabrics from low bioturbation indices and deep tiers to completely bioturbated. The resulting ichnofabrics are plotted against depth and can directly be compared to spectral natural gamma ray logs, which in the discussed example are dominated by variations of the uranium content reflecting the organic matter content in the sediment. The ichnofabric analysis of carbonate sediment cores of the Maldives, recovered during IODP Expedition 359, demonstrates a good correlation between synthetic ichnofabric logs and downhole gamma radiation logs. The combined study of these logs provides information on the main changes in the organic matter content of the sediment. The graphical representation of ichnofabrics together with gamma ray logs presented here is a very useful implement for sedimentologists working on cores.

Keywords: ichnology; bioturbation; downhole logging; Natural gamma-ray logs; Oligocene-Miocene; Maldives; IODP Expedition 359.

Introduction

Ichnofabric analysis is an excellent tool for the study of sediment cores (Taylor et al., 2003; Gerard and Bromley, 2008; Buatois and Mángano, 2011; Ekdale et al., 2012). It is based on the integration of different data, including the original sedimentary characteristics together with features of biodeformation (Taylor et al., 2003; Buatois and Mángano, 2011; Ekdale et al., 2012). The definition of ichnofabrics relies on the description of the ichnological composition (diversity, size, tiering, and cross-cutting relationship of ichnotaxa), the intensity of the bioturbation, as well as sedimentological aspects such as grain size, texture, and composition (Taylor et al., 2003; McIlroy, 2004, 2007, 2008; Rodríguez-Tovar and Dorador, 2015). Taphonomy has to be considered because factors such as erosion, compaction, and diagenetic effects may have significant impact upon the preserved ichnoassemblages (Hallan, 1975). All these parameters provide information on paleoecological and depositional conditions during sedimentation and make the ichnofabric analysis a useful tool for paleoenvironmental interpretations, basin analysis, or even reservoir characterization (Knaust, 1998; Buatois and Mángano, 2011; Ekdale et al., 2012; Giraldo-Villegas et al., 2016; Rodríguez-Tovar et al., 2017). Oxygen-influenced ichnofabrics are especially relevant to aid in the exploration for unconventional hydrocarbon resources, which are of strong economic interest (Bockelie, 1991; Schieber, 2003; Ekdale et al., 2012).

Where no cores are retrieved from wells, downhole logs are used to define physical, compositional, and structural properties of the formation. Data can be used for characterizing the geochemical composition, mineralogy, lithology, and stratigraphy of the deposits. At drill sites with a good core recovery, log and core data complement one another. This study therefore proposes a unifying way to organize and visualize ichnofabrics. This allows the integration of ichnological data, downhole logs, and core physical properties. The ichnofabric analysis of the IODP 359 cores from the Maldives results in synthetic logs that are directly comparable to those of the natural gamma radiation.

Material and methods

IODP Exp. 359 Site U1468 is located in the Kardiva Channel of the Maldives Inner Sea (4°55.98'N; 73°4.28'W). The well penetrated an Oligocene to Pleistocene succession with a variety of facies and trace fossils (Betzler et al., 2016, 2017, 2018; Fig. 1).

The recovered core sections at Site U1468 were run through the Natural Gamma Radiation Logger (NGRL). The NGRL measures the natural emission of uranium (^{238}U), thorium (^{232}Th), and potassium (^{40}K) on whole-round cores at sample positions 10 cm apart for the total 150-cm-length of section. The NGR spectroscopy measures a wide energy spectrum that was used to estimate the abundance of each isotope based on the strength of the signal at characteristic energies (Blum et al., 1997; Gilmore, 2008). Spectral data were collected for post-cruise processing of U, Th, and K abundance following the methodology proposed by De Vleeschouwer et al. (2017).

Downhole gamma ray logging was performed at Site U1468. The Schlumberger Hostile Environment Natural Gamma Ray Sonde (HNGS) has a vertical resolution of 30 cm (Betzler et al., 2017). The HNGS is a spectral log determined by the concentrations of K (in weight percent), and Th and U (in parts per million) from the representative gamma ray energies of the isotopes of their radioactive-decay series, which dominate the natural radiation spectrum. The HNGS also measures the total gamma ray (HSGR) radiation in American Petroleum Institute units (gAPI). The HNGS response is influenced by the borehole diameter and by the presence of bentonite and KCl in the drilling mud, and therefore the measurements are corrected for the borehole diameter variations and for the drilling mud gamma ray energies (Betzler et al., 2017). The ichnofabric analysis was conducted on cores and on high-resolution images of core section halves. According to reflection seismic profiles, sedimentological data, and the biostratigraphy presented by Betzler et al. (2016, 2017, 2018), the ichnofabric analysis was focused on slope to basinal deposits encompassing the Oligocene (Chattian) to Middle Miocene (Serravallian) (Fig. 1). This environment was generally stable at the time of deposition, punctuated by rare episodic gravity flows. The cores mostly consist of hemipelagic-pelagic carbonates with abundant planktic foraminifera and diverse platform-derived bioclasts. The materials are intensely bioturbated. The siliciclastic content at the study site is very low because of the isolation of the Maldives from river input (Betzler et al., 2017).

Approach

The proposed ichnofabric analysis is a combination of classical sedimentological and ichnological approaches developed by others authors elsewhere (Droser and Bottjer, 1986; Bromley, 1996; Taylor et al., 2003; Hansen and MacEachern, 2007; Dorador et al., 2014ab; Rodríguez-Tovar and Dorador, 2015), that has been organized in three steps to integrate all the information in a synthetic ichnofabric log. The first two steps are a summary of the classical working flow in ichnology and sedimentology. The third step organizes and displays the ichnofabric information in a way which in the example herein discussed characterizes the organic content of the carbonates.

Step 1: Core analysis.

This first step consists of the ichnological core analysis and is carried out directly on core and also on high resolution photographs of the core halves (Fig. 2). To achieve a good contrast of sediment textures, core analysis may be preceded by adequate water impregnation for lithified sediments and by smoothing of the surface of unlithified deposits. The analysis of core photographs is recommended as it allows the digital enhancement of the image in order to improve the visibility of biogenic structures (Dorador et al., 2014a; Rodríguez-Tovar and Dorador, 2015). The quantification of the bioturbation intensity follows the method of Taylor and Goldring (1993), Taylor et al. (2003), and Hansen and MacEachern (2007). Identification of the main ichnotaxa, measurement of the burrow sizes, of the depth of burrowing or tiering, and cross-cutting relationships were also recorded. The estimation of the abundance of the different ichnotaxa and the degree of mottling can be obtained: (1) visually, by direct comparison with percentage diagrams or flash cards (Droser and Bottjer, 1986), (2) semiquantitatively after using point-counting grids (as used in clastic sediments by Heard et al., 2014), or (3) by estimation of pixel amounts with Adobe Photoshop or JMicroVision (Roduit, 2006; Dorador et al., 2014b). The compilation of these different data results in the characterization of the different ichnoassemblages in the core.

Step 2: Ichnofabric definition.

During this step the different ichnofabrics are defined. First the bioturbation index is considered in order to differentiate core segments with different burrowing intensity. Once the different segments are established, the focus is on the ichnoassemblages. As in classical facies or microfacies analysis, the different components of the assemblage are listed in order of abundance using qualitative scales (abundant, common, frequent, rare, present, Table 1) or according to the quantitative values obtained with digital methods. The core thus will be divided into segments defined by the type and intensity of burrowing. This classification has to be linked to the available sedimentological information, i.e., sediment texture, grain size, and composition (Table 1). The ichnofabrics can therefore be defined according to the bioturbation index, the ichnoassemblage, and the sediment type. If needed, to manage a reasonable amount of ichnofabrics, several fabrics can be merged together according to their main features.

Step 3: Ichnofabric organization.

Prior to their graphical representation, the different ichnofabrics are sorted. In general terms, the ichnofabrics with lower bioturbation indices and deeper tiers are typically related to restricted oxygen conditions that can be ultimately linked to the organic matter content (Savrda and Bottjer, 1986, 1989). Using this assumption, for example a succession of ichnofabrics can be established that reflects the organic content of the sediment. To achieve this objective it is proposed to organize the ichnofabrics using three criteria; (1) the ichnofabrics have to be ordered according to an increasing bioturbation index, as in the diagrams for bioturbation indices by Droser and Bottjer (1986); (2) for the ichnofabrics with the same bioturbation index those with deeper tiers are considered as indicative of sediment with a higher organic content. The tiering diagrams proposed by Bromley (1996) can be used to achieve this differentiation; and (3) for the ichnofabrics with identical bioturbation indices and tiering, the sediment texture and grain size are used as proxies for the energy of the environment that may exert at least a passive control on the oxygenation and organic content (Table 2). Therefore, the resulting ichnofabric order, which summarizes the combined information of bioturbation intensity, tiering, and sediment texture can be numbered, numbers reflecting the inferred degrees of oxygenation at the sea floor.

This representation is similar to the one proposed by Droser and Bottjer (1988, 1993) and Bottjer and Droser (1991) for ichnofabric indices. There are also examples of ichnofabric representation in carbonates in order to reconstruct palaeoenvironments (Knaust, 1998) or even the relative oxygenation (Giraldo-Villegas et al., 2016). Here, this approach can be tested and amended by corroborating the interpretation through a correlation with the gamma ray logs directly reflecting the organic content of the sediment.

Results

Ichnofabrics

The approach described herein was applied to the carbonate platform slope and basinal sediments of IODP Exp. 359 Site U1468 (Fig. 1). The nature of the carbonate sediment may display a low contrast in color that may complicate ichnotaxa identification and bioturbation quantification (Cummings and Hodgson, 2011). This may have locally affected the identification of *Scolicia* or other echinoid-related traces that are otherwise common burrowers in carbonate environments (Uchman, 2007; Cummings and Hodgson, 2011).

The studied section at Site U1468 has a core recovery of 43% and is up to 430 m thick. The ichnofabric analysis was conducted in every 1.5 m section of a core (Fig. 2), however for the complete 10-m length of the core just the two main ichnofabrics are represented for improving the graphical representation. For an optimal visualization the total amount of ichnofabrics at Site U1468 was reduced to nine (Table 2, Fig. 3). The ichnofabrics were plotted against depth (Fig. 4).

The ichnofabric log for Site U1468 shows a clear trend of ichnofabrics with an up-core increasing bioturbation index. The lower interval (850 meters below sea floor to 820 mbsf) contains ichnofabrics with a high bioturbation index (IF1 and 6), with the exception of a weakly bioturbated interval with IF9 in core 108R (Fig. 4, Table 2). In the overlying interval (820 mbsf to 720 mbsf), there is an alternation of ichnofabrics with a low (IF9 and 8) and a high bioturbation index (IF6, Fig. 4). The main ichnotaxa in the low-bioturbation intervals are *Planolites* and *Phycosiphon* as upper tiers, *Thalassinoides* and *Planolites* as middle tiers, and *Chondrites* as deep tiers. The intensely bioturbated parts have a mottled texture and additionally present *Palaeophycu*s as upper tier and *Zoophycos* as deep tier ichnotaxa.

The overlying interval (720 mbsf to 602 mbsf) starts with an alternation of IF7 and IF8. Up-core there is a thick package characterized by IF5 which intercalates with convolute beds without any bioturbation, and intervals with IF3 and IF7. At 602 mbsf, there is a sharp change from IF7 to IF3 marked by a sudden increase in the intensity of bioturbation (Fig. 4). Up-section, there is a gradual change from IF3 to alternating IF2 and IF4. The bioturbation index in this part of the succession is high and single burrows are difficult to distinguish.

Natural Gamma Radiation

From 800 mbsf up to 720 mbsf there are relatively low baseline values (~9 gAPI), however, the gamma ray profile in this interval exhibits the greatest variability (from 8 to 86 gAPI, Fig. 5). The spectral data show values close to zero for K and Th, while the U content averages 2 ppm, with maximal concentrations around 10 ppm (Fig. 5). At 720 mbsf, there is an increase in the gamma ray values, and the amplitude of variations is still high to 602 mbsf. From 602 mbsf to 490 mbsf the amplitude gradually decreases and the profile ranges from low- to moderate-amplitude variability, with values between 16 to 54 gAPI and 2 to 3.8 ppm of U. The interval between 490-450 mbsf is marked by a change in the character of the gamma ray log, with multiple sharp peaks of elevated gamma ray (up to 43 gAPI; 5 ppm of U). From 450 mbsf to 430 mbsf, there is a new reduction on the average values of the gamma ray (~10 gAPI).

There is good consistency between NGR measurements and the gamma ray log from the spectral tool (HNGS) (Fig. 5). Although it is difficult to match specific peaks and lows given the incomplete core recovery, similar trends are observed and a few distinctive features can be correlated, such as for example, the interval of high gamma ray between 720 and 730 mbsf. The NGR values at the bottom of the hole are low (<20 counts/s) with a first high peak at ~807 mbsf. From there up to 720 mbsf there is an alternation of organic-rich black and organic-poor white sediment layers which are represented respectively by high and low NGR values. The interval of relatively constant gamma ray values between 480 and 602 mbsf is also recorded by the NGR. The uppermost part of the platform slope sequence, between 430-480 mbsf, shows a great variability and ranges from ~10 to 40 counts/s with no apparent trend.

Discussion and Conclusions

At IODP Site U1468 the natural gamma logs are indicative of organic matter content in the sediment (Betzler et al., 2016). Spectral gamma ray data show that uranium is the primary contributor to the total gamma-ray variability (Fig. 5). Potassium and thorium are only accessories and sometimes below the detection limit. Uranium is typically reduced by organic matter and its amount is therefore directly proportional to the quantity of available organic matter (Leventhal et al., 1986).

Lithology exerts a control to a certain extent as sediment texture, grain size, and sorting may determine the accumulation and preservation of organic matter in the sediment, and accordingly the possible ichnological assamblage. In the study section there is a primary control exerted by lithology on ichnofabrics where coarser materials have intensely bioturbated ichnofabrics and vice versa (Fig. 4). There is no clear link between lithology and diversity of trace fossils. The mudstone and the floatstone intervals display similar diversity, but they present completely different intensity of bioturbation (Table 1). In the study section there is a locally consistent correlation between texture/grain size and the HSGR and NGR. However, such consistency disappears when the complete succession is considered. Some coarse-grained intervals (i.e. packstone-grainstone texture) seem to correlate to high gamma ray values. Finer intervals (i.e. wackestone and mudstone texture) locally correlate to low gamma ray values, but this correlation is not univocal and wackestone-mudstone intervals may display values similar or even higher than those of the coarse-grained intervals (Fig. 5).

For the succession there is a clear correlation between the gamma ray log and the ichnofabric log generated by the herein adopted methodology. The main shifts in the gamma ray logs, also recorded by the NGR, have equivalent shifts in the ichnofabric logs at 820 mbsf, 720 mbsf, and

602 mbsf. The interval with relatively constant gamma ray values between 602 mbsf and 490 mbsf has a clear counterpart in the ichnofabric log. There are also distinctive gamma ray peaks at 570 and 535 mbsf that are also recorded by the ichnofabric log. Accordingly, it is proposed that the herein developed graphical representation of ichnofabrics can be used as an approximation to the organic-matter content of the sediment.

As an illustrative example, the occurrence of black organic-rich sediments alternating white organic-poor sediments at the bottom of the succession (Fig. 4, IF9-7) can be used as a calibration for the relation between organic content, gamma radiation, and ichnofabrics (Fig. 6). The black-sediment layers have a total organic content (TOC) of up to 8 % (Betzler et al., 2016, 2018) and are the ones with the highest NGR gamma ray values in the section analyzed (Fig. 6). They contain the ichnofabrics with the lowest bioturbation indices (IF 9 and IF8) and the smallest burrows. Small burrows are invoked as sign of environmental stress such as increased fluvial input or rapid deposition (MacEachern et al., 2007), but such stress factors can be discarded in the case of the Maldives. The studied materials are interpreted as a distal slope setting where the sedimentation was stable, dominantly hemipelagic rain, without fluvial influence (Betzler et al., 2016, 2018). According to Uchman and Wetzel (2011) and Wetzel and Uchman (2012) small sized burrows, low amount of tiers, and low bioturbation intensity, as those observed in the black layers, are distinctive of reduced oxygenation either of the bottom water or inside the sediment. The authors also report such ichnofabric features as indicative of high content in organic matter in the sediment. Both, seafloor oxygenation and organic-matter content in the sediment are closely related. The oxygenation of the sea floor may depend on the amount of organic matter being deposited at the seafloor that may change the depth of the redox boundary (Wetzel, 2010; Wetzel and Uchman, 2012). Thus, according to the nature of the sediment and the depositional environment of the study case, the low bioturbation indices and small burrows are interpreted as clear indicators of both reduced oxygenation and high content in organic matter (Taylor et al., 2003; Gerard and Bromley, 2008). The high uranium content in this case is therefore consistent with the interpretation of black layers as organic-rich materials deposited during periods of higher productivity or a period with a reducing poorly-oxygenated depositional environment (Leventhal et al., 1986).

The contribution to the total gamma radiation of the potassium and thorium is very limited (Fig. 5) due to the exceptional location of the Maldives which is protected from intense detrital input of minerals rich in these elements (Betzler et al., 2016). In other sedimentary environments with greater terrigenous input, the total natural gamma radiation is expected to be a combination of the K, Th, and U. In such a scenario, the proposed ichnofabric methodology may help in the recognition of variations in the organic matter content, that otherwise will be masked by the stronger signals of K and Th.

In summary, the ichnofabric logging method presented here is a very useful implement for sedimentologists working on cores. The methodology provides preliminary but accurate environmental information, especially on the oxygenation and/or organic matter content of the sea floor. The resulting ichnofabric log parallels the spectral natural gamma radiation log dominated by uranium, a typical indicator of organic matter content in the sediment. In sediment cores with higher siliciclastic content, the proposed ichnofabric methodology may help in the recognition of variations in the organic matter content, that otherwise will be masked by the stronger signals of K and Th. The synthetic ichnofabric logs may also be of the greatest interest for those drilling sites where downhole logging include imaging tools as 360° optical and acoustic televiewers. Such tools provide a continuous record of the bore hole by spatially-oriented high-resolution images that ichnologists and sedimentologists can use for the characterization of the sedimentary formations.

Acknowledgements

We acknowledge funding by the DFG through grant Be 1272/23-1. Many discussions with the IODP Exp. 359 shipboard scientists helped us to sharpen our concept; special thanks go to

Gregor Eberli and Angela Slagle. The authors want to thank editor Luis Buatois and two anonymous reviewers for their valuable comments.

References

Betzler, C., Eberli, G.P., Kroon, D., Wright, J.D., Swart, P.K., Nath, B.N., Alvarez-Zarikian, C.A., Alonso-García, M., Bialik, O.M., Blättler, C.L., Guo, J.A., Haffen, S., Horozal, S., Inoue, M., Jovane, L., Lanci, L., Laya, J.C., Mee, A.L.H., Lüdmann, T., Nakakuni, M., Niino, K., Petruny, L.M., Pratiwi, S.D., Reijmer, J.J.G., Reolid, J., Slagle, A.L., Sloss, C.R., Su, X., Yao, Z., Young, J.R., 2016. The abrupt onset of the modern South Asian Monsoon winds. Scientific Reports 6:29838. http://dx.doi.org/10.1038/srep29838.

Betzler, C., Eberli, G.P., Alvarez Zarikian, C.A., and the Expedition 359 Scientists, 2017. Maldives Monsoon and Sea Level. Proceedings of the International Ocean Discovery Program, 359: College Station, TX (International Ocean Discovery Program). http://dx.doi.org/10.14379/iodp.proc.359.2017.

Betzler, C., Eberli, G.P., Lüdmann, T., Reolid, J., Kroon, D., Reijmer, J.J.G., Swart, P.K., Wright, J.D., Young, J.R., Alvarez-Zarikian, C.A., Alonso-García, M., Bialik, O.M., Blättler, C.L., Guo, J.A., Haffen, S., Horozal, S., Inoue, M., Jovane, L., Lanci, L., Laya, J.C., Mee, A.L.H., Nakakuni, M., Nath, B.N., Niino, K., Petruny, L.M., Pratiwi, S.D., Slagle, A.L., Sloss, C.R., Su, X., Yao, Z., 2018. Refinement of Miocene sea level and monsoon events from the sedimentary archive of the Maldives (Indian Ocean). Progress in Earth and Planetary Science 5. DOI 10.1186/s40645-018-0165-x.

Blum, P., 1997. Technical Note 26: Physical Properties Handbook—A Guide to the Shipboard Measurement of Physical Properties of Deep-Sea Cores. Ocean Drilling Program. http://dx.doi.org/10.2973/odp.tn.26.1997.

Bockelie, J.F., 1991. Ichnofabric mapping and interpretation of Jurassic reservoir rocks of the Norwegian North Sea. Palaios 6, 206–215. DOI: 10.2307/3514902.

Bottjer, D.J., Droser, M.L., 1991. Ichnofabric and basin analysis. Palaios 6, 199–205.

Bromley, R.G., 1996. Trace Fossils; Biology, Taphonomy and Applications, 2nd edn. Chapman & Hall, London.

Buatois, L.A., Mángano, M.G., 2011. Ichnology: Organism-Substrate Interactions in Space and Time, Cambridge University Press, New York.

Cummings, J.P., Hodgson, D.M., 2011. Assessing controls on the distribution of ichnotaxa in submarine fan environments, the Basque Basin, Northern Spain. Sedimentary Geology 239, 162–187. https://doi.org/10.1016/j.sedgeo.2011.06.009.

De Vleeschouwer, D., Dunlea, A.G., Auer, G., Andreson, C.H., Brumsack, H., de Loach, A., Gurnis, M., Huh, Y., Ishiwa, T., Jang, K., Kominz, M.A., März, C., Schnetger, B., Murray, R. W., Pälike, H., and Expedition 356 Shipboard Scientists, 2017. Quantifying K, U, and Th contents of marine sediments using shipboard natural gamma radiation spectra measured on DV JOIDES Resolution. Geochemistry, Geophysics, Geosystems 18, 1053–1064. DOI: 10.1002/2016GC006715.

Dorador, J., Rodríguez-Tovar, F.J., and IODP Expedition 339 Scientists, 2014a. Digital image treatment applied to ichnological analysis of marine core sediments. Facies 60, 39–44. DOI: 10.1007/s10347-013-0383-z.

Dorador, J., Rodríguez-Tovar, F.J., and IODP Expedition 339 Scientists, 2014b. Quantitative estimation of bioturbation based on digital image analysis. Marine Geology 349, 55–60. http://dx.doi.org/10.1016/j.margeo.2014.01.003.

Droser, M.L., Bottjer, D.J., 1986. A semiquantitative field classification of ichnofabric. Journal of Sedimentary Petrology 56, 558–559. DOI: 10.1306/212F89C2-2B24-11D7-8648000102C1865D.

Droser, M.L., Bottjer, D.J., 1988. Trends and extent of bioturbation in Cambrian carbonate marine environments, western United States. Geology 16, 233–236.

Droser, M.L., Bottjer, D.J., 1993. Trends and patterns of Phanerozoic ichnofabrics: Annual Review of Earth and Planetary Sciences 21, 204–225.

Dunham, R.J., 1962. Classification of carbonate rocks according to depositional texture, in Ham, W.E. (Ed.), Classification of Carbonate Rocks. AAPG Memoir 1, 108–121. http://archives.datapages.com/data/specpubs/carbona2/data/a038/a038/0001/0100/0108.htm.

Ekdale, A.A., Bromley, R.G., Knaust, D., 2012. The ichnofabric concept. Trace Fossils as Indicators of Sedimentary Environments. Developments in Sedimentology 64, 139–155.

Embry, A.F., Klovan, J.E., 1972. Absolute water depth limits of late Devonian ecological zones. Geologische Rundschau 61, 672–686. http://dx.doi.org/10.1007/BF01896340.

Gerard, J., Bromley, R., 2008. Ichnofabrics in Clastic Sediments: Application to Sedimentological Core Studied, ed. Gerard, Madrid.

Gilmore, G.R., 2008. Practical Gamma-ray Spectrometry, ed. John Wiley & Sons, Hoboken. http://dx.doi.org/10.1002/9780470861981.

Giraldo-Villegas, C.A., Celis, S.A., Rodríguez-Tovar, F.J., Pardo-Trujillo, A., Vallejo-Hincapié, D.F., Trejos-Tamayo, R.A., 2016. Ichnological analysis of the Upper Miocene in the ANH-Tumaco-1-ST-P well: assessing paleoenvironmental conditions at the Tumaco Basin, in the Colombian Pacific. Journal of South American Earth Sciences 71, 41–53. http://dx.doi.org/10.1016/j.jsames.2016.06.008.

Hallam, A., 1975. Preservation of Trace Fossils, in: Frey R.W. (Ed.), The Study of Trace Fossils. Springer, Berlin. https://doi.org/10.1007/978-3-642-65923-2_4.

Hansen, C.D., MacEachern, J.A., 2007. Application of the asymmetric delta model to along-strike facies variations in a mixed wave- and river-influenced delta lobe, Upper Cretaceous Basal Belly River Formation, central Alberta, in: MacEachern, J.A., Bann, K.L., Pemberton, S.G. (Eds.), Applied Ichnology. SEPM Short Course Notes 52, pp. 256–272.

Heard, T.G., Pickering, K.T., Clark, J.D., 2014. Ichnofabric characterization of a deep-marine clastic system: a subsurface study of the Middle Eocene Ainsa System, Spanish Pyrenees. Sedimentology, 61, 1298–1331. DOI: 10.1111/sed.12101.

Knaust, D., 1998. Trace fossils and ichnofabrics on the Lower Muschelkalk carbonate ramp (Triassic) of Germany: tool for high-resolution sequence stratigraphy. Geologische Rundschau 87, 21–31.

MacEachern, J.A., Pemberton, S.G., Gingras, M.K., Bann, K.L., Dafoe, L.T., 2007. Use of trace fossils in genetic stratigraphy, in: Miller, W. (Ed.), Trace Fossils. Concepts, Problems, Prospects. Elsevier, Amsterdam, pp. 105–128.

McIlroy, D., 2004. Some ichnological concepts, methodologies, applications and frontiers, in: McIlroy, D. (Ed.), The Application of Ichnology to Palaeoenvironmental and Stratigraphic Analysis. Special Publication of the Geological Society, 228, 3–29.

McIlroy, D., 2007. Lateral variability in shallow marine ichnofabrics: implications for the ichnofabric analysis method. Journal of the Geological Society, 164, 1–11.

McIlroy, D., 2008. Ichnological analysis: The common ground between ichnofacies and ichnofabric analysts. Palaeogeography, Palaeoclimatology, Palaeoecology, 270, 332–338.

Leventhal, J.S., Daws, T.A., Frye, J.S., 1986. Organic geochemical analysis of sedimentary organic matter associated with uranium. Applied Geochemistry, 1, 241–247. https://doi.org/10.1016/0883-2927(86)90008-9.

Rodríguez-Tovar, F.J., Dorador, J., 2015. Ichnofabric characterization in cores: a method of digital image treatment. Annales Societatis Geologorum Poloniae, 85, 465–471. http://dx.doi.org/10.14241/asgp.2015.010.

Rodríguez-Tovar, F.J., Dorador, J., Mayoral, E., and Santos, A., 2017. Outcrop and core integrative ichnofabric analysis of Miocene sediments from Lepe, Huelva (SW Spain): Improving depositional and paleoenvironmental interpretations. Sedimentary Geology, 349, 62–78. DOI: 10.1016/j.sedgeo.2017.01.001.

Roduit, N., 2006. JMicroVision: Image analysis toolbox for measuring and quantifying components of high-definition images. Version 1.2.2. http://www.jmicrovision.com (accessed 2 July 2006).

Savrda, C.E., Bottjer, D.J., 1986. Trace fossil model for reconstruction of palaeo-oxygenation in bottom-waters. Geology, 14, 3–6. https://doi.org/10.1130/0091-7613(1986)14<3:TMFROP>2.0.CO;2.

Savrda, C.E., Bottjer, D.J., 1989. Anatomy and implications of bioturbated beds in ‘black shale’ sequences: examples from the Jurassic Posidonienschiefer (southern Germany). Palaios, 4, 330–342. DOI: 10.2307/3514557.

Scheiber, J., 2003. Simple gifts and buried treasures–implications of finding bioturbation and erosion surfaces in black shales. The Sedimentary Record, 1, 4–8. DOI: 10.4236/ijg.2016.712099.

Taylor, A.M., Goldring, R., 1993. Description and analysis of bioturbation and ichnofabric. Journal of the Geological Society, 150, 141–148. DOI: 10.1144/gsjgs.150.1.0141.

Taylor, A.M., Goldring, R., Gowland, S., 2003. Analysis and application of ichnofabrics. Earth Science Reviews, 60, 227–259. https://doi.org/10.1016/S0012-8252(02)00105-8.

Uchman, A., 2007. Deep-sea ichnology: development of major concepts, in: Miller, W. (Ed.), Trace fossils. Concepts, problems, prospects. Elsevier, Amsterdam, pp. 248–267.

Uchman, A., Wetzel, A., 2011. Deep-sea ichnology: the relationships between depositional environment and endobenthic organisms, in: Hüneke, H., Mulder, T. (Eds.), Deep-Sea Sediments. Developments in Sedimentology, Elsevier, Amsterdam, pp. 517–556.

Wetzel, A., 2010. Deep-sea ichnology: observations in modern sediments to interpret fossil counterparts. Acta Geologica Polonica 60, 125–138.

Wetzel, A., Uchman, A., 2012. Hemipelagic and pelagic basin plains, in: Bromley, R.G., Knaust, D. (Eds.), Trace Fossils as Indicators of Sedimentary Environments. Developments in Sedimentology 64, Elsevier, Amsterdam, pp. 673–701.

Figures

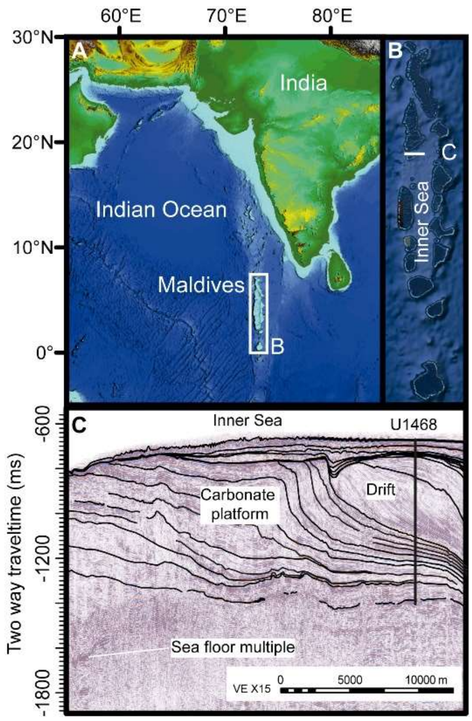

Figure 1: **A** Location of the Maldives in the Indian Ocean. **B** Close up of the Maldives showing the Inner sea bounded by a double raw of atolls. **C** Seismic line NEOMA-P65 cross cutting the Kardiva Channel. The black lines stand for the lower boundaries of the platform and drift sequences. Age after Betzler et al. (2017, 2018).

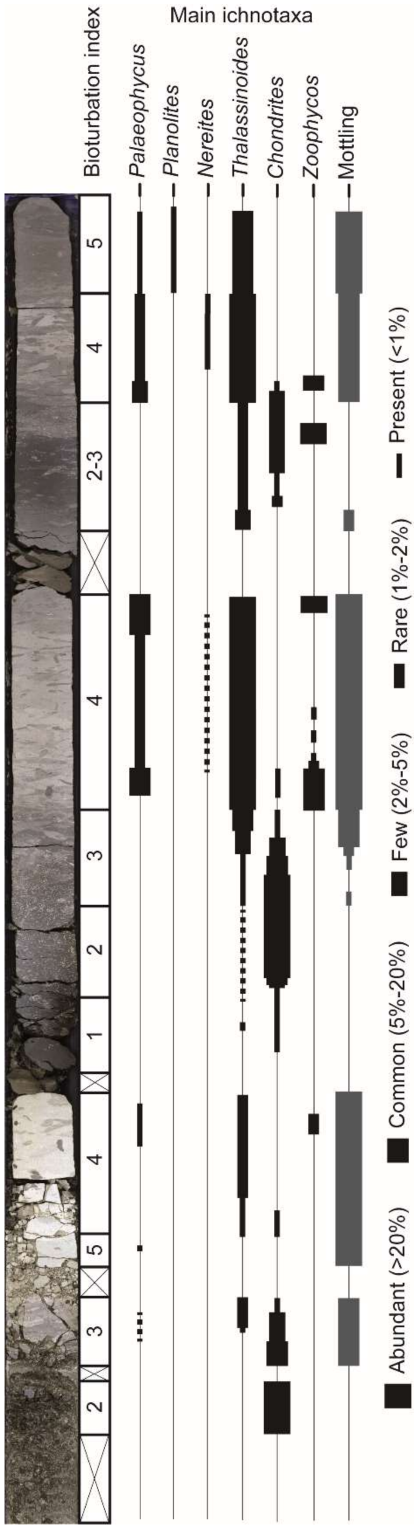

Figure 2: Step 1. The enhanced photograph is used to analyze the intensity of bioturbation (From 1-6 according to Hansen and MacEachern, 2007) and the abundance of each ichnotaxa. The intervals with drilling disturbances are marked with crosses in the column of the bioturbation index.

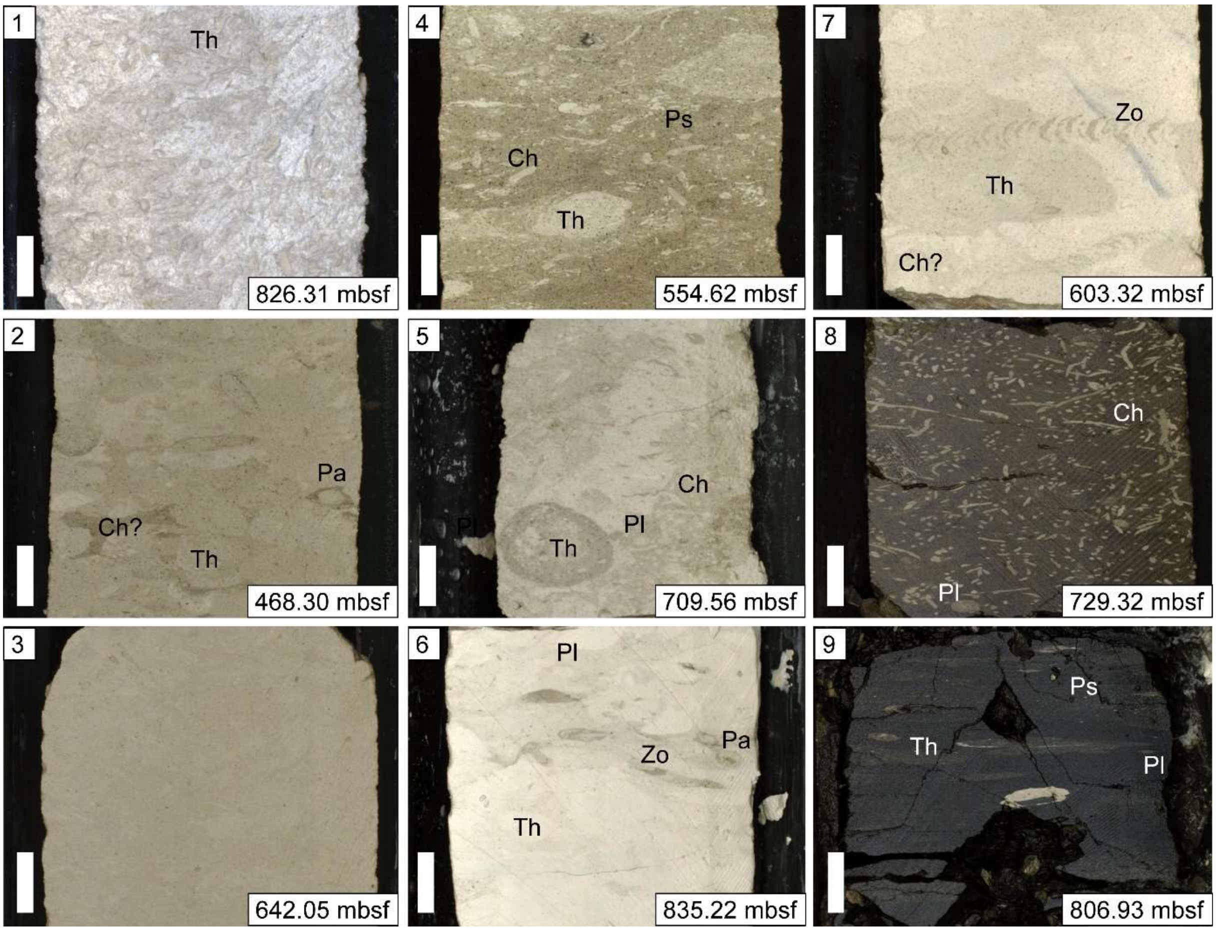

Figure 3: Ichnofabrics (IF1 to IF9) at IODP Site U1468. The main ichnotaxa in these ichnofabrics are *Chondrites* (Ch), *Nereites* (Ne), *Palaeophycus* (Pa), *Phycosiphon* (Ps), *Planolites* (Pl), *Thalassinoides* (Th), and *Zoophycos* (Zo). Given depths in meters below the sea floor (mbsf) for the top of the images. Some *Thalassinoides* (i.e those of IF4) may be echinoid related traces, but the nature of the sediment did not allow any further identification. Length of white bar: 1 cm.

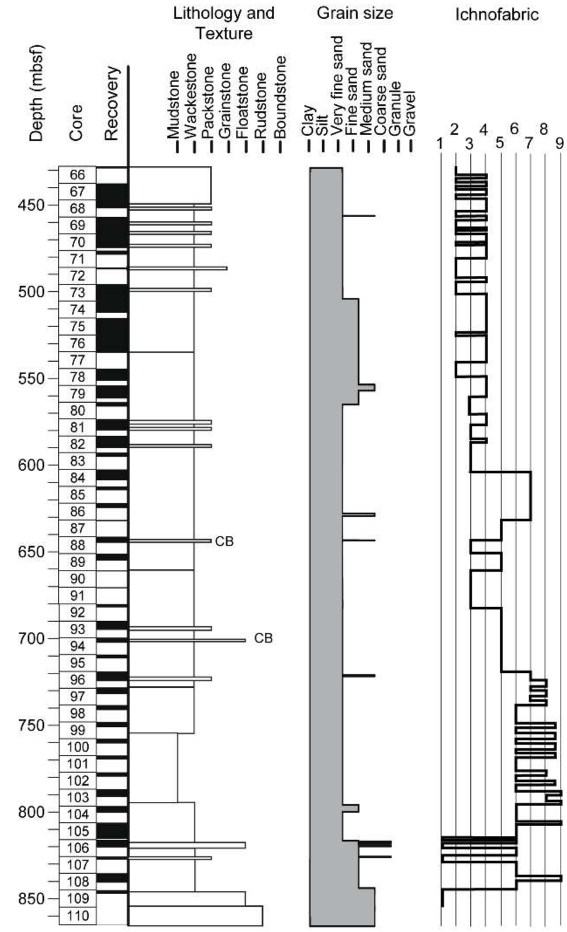

Figure 4: Lithological column of the basin to slope deposits at IODP Site U1468. The figure includes from left to right the depth (mbsf), core number, core recovery, sediment texture after Dunham (1962) and Embry and Clovan (1974), grain size of bioclasts and components after Wentworth (1922), and ichnofabrics (See Fig. 3 and Table 2). CB= Convolute beds.

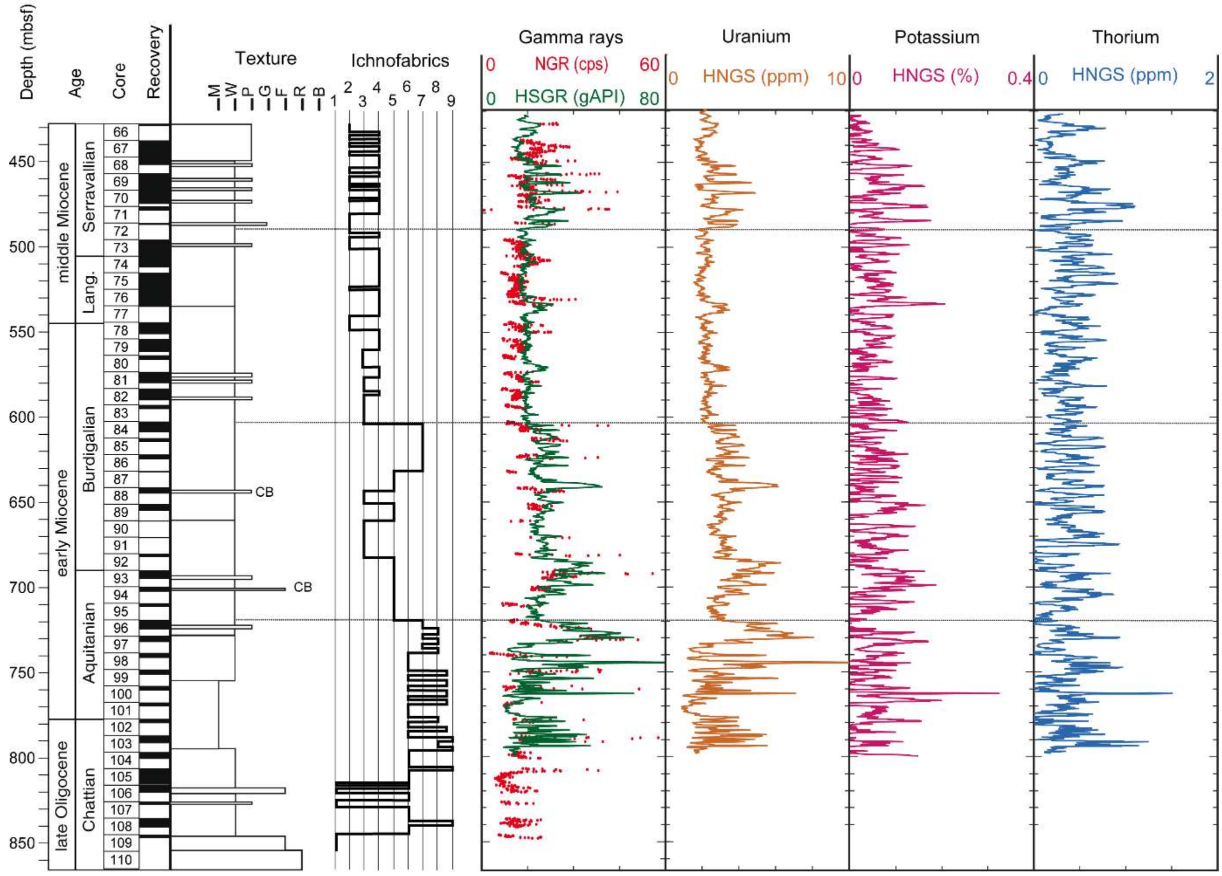

Figure 5: Natural gamma radiation measurements at IODP Site U1468. From left to right: depth (mbsf), age after Betzler et al. (2017, 2018), core, recovery, sediment texture, ichnofabrics (IF1 to IF9), gamma ray measurements in core (NGR), downhole (HSGR), and spectral gamma radiation by uranium, potassium and thorium (downhole). The plot with the total gamma radiation also displays the ichnofabric log with dashed line in the background. The HSGR perfectly mirrors the spectral radiation by the uranium. Potassium and thorium contribution is almost not significant. The horizontal dashed lines are guidelines to divide the different intervals characterized by their gamma radiation and ichnofabrics (See discussion in text). CB= Convolute beds.

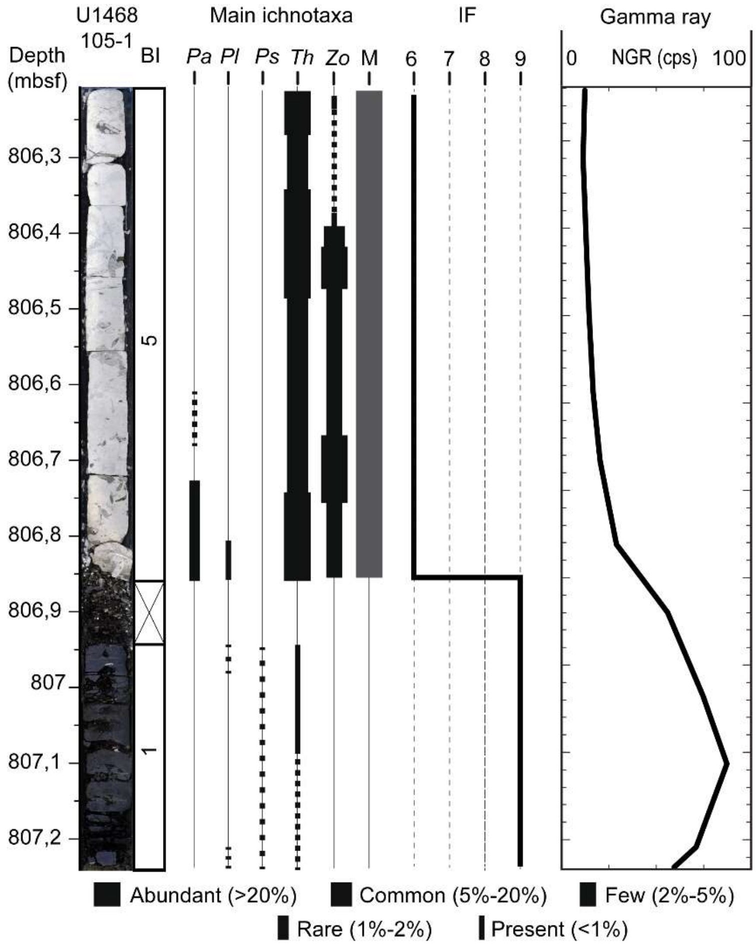

Figure 6: Example of the alternation of black- and white-sediment intervals from IODP Site U1468-105X-1. From left to right: depth (mbsf), core photograph, bioturbation index (BI), abundance of the main ichnotaxa (*Palaeophycus*-Pa, *Planolites*-Pl, *Phycosiphon*-Ps, *Thalassinoides*-Th, and *Zoophycos*-Zo) and mottling (M), ichnofabrics (IF6 to IF9, see Table 2), and natural gamma radiation including total counts per second (NGR). The interval with drilling disturbances is marked with a cross in the BI column.

IODP Exp 359 Cores	Bioturbation index	*Palaeophycus*	*Phycosiphon*	*Planolites*	*Nereites*	*Thalassionides*	*Chondrites*	*Zoophycos*	Texture
359-U1468A-66X	6					1			P
359-U1468A-67X	5		1			2	1		P
359-U1468A-68X	4-5		2	1		3	2		P
359-U1468A-69X	6		1			1			P-W
359-U1468A-70X	5		2	1		3	2		P-W
359-U1468A-71X	4-5		2	2		3	2	1	W
359-U1468A-72X	6								P
359-U1468A-73X	5-6	1	1	1		1	1	1	P-W
359-U1468A-74X	5	1	1	2		3	4		W-P
359-U1468A-75X	4-5			2	1	3	3		W-P
359-U1468A-76X	5			2		3	3		W-P
359-U1468A-77X	4-5	1		1	1	5	4		W-P
359-U1468A-78X	3	4	1	3	2	5	1		W-P
359-U1468A-79X	4		2			4	3	3	P-W
359-U1468A-80X	5-6	2	1	1		3			W-P
359-U1468A-81X	4-5	4	2	3	2	5	1		P-W
359-U1468A-82X	5-6	4	1	3	2	5	1		P-W
359-U1468A-83X	5-6			1		2			W
359-U1468A-84X	5	1		1	2	4	3	4	W
359-U1468A-85X	4-3	1		1	2	4	3	4	W
359-U1468A-86X	5	1		1	2	4	3	4	W
359-U1468A-87X	4	3		1		5	4	1	W
359-U1468A-88X	5-6					3	1		W-P
359-U1468A-89X	4	3		1		5	4	1	W
359-U1468A-90X	5-6			1		2			W
359-U1468A-91X	5-6			1		2			W
359-U1468A-92X	6					1			W
359-U1468A-93X	4-5	4	1	3	2	5	1		W-P
359-U1468A-94X	5					4	2		W-P
359-U1468A-95X	4-5	1		1	1	5	4		W
359-U1468A-96X	5			1		2			W
359-U1468A-97X	1-2		1	1		2	3		W
359-U1468A-98X	4-5	3		1		5	4	1	W
359-U1468A-99X	1-2		1	1		2	2		W
359-U1468A-100X	1-2					2			W-M
359-U1468A-101X	4-5	3		2	2	4	2	2	W-M
359-U1468A-102X	1-2			1		2	1		W-M
359-U1468A-103X	1-2		1	1		2	2		W
359-U1468A-104X	4-5		1			5		4	W-M
359-U1468A-105X	4-5		1	1		4		5	W
359-U1468A-106X	6					1			F
359-U1468A-107X	4-5			1	1	3	1		W-F
359-U1468A-108X	4-5	3	2	1	1	4	2		W
359-U1468A-109X	6					1			F

Table 1: Core-by-core summary of the main features for ichnofabric definition: bioturbation index (after Hansen and MacEachern, 2007), relative abundance of the different ichnotaxa (from abundant-5 to present-1, see Figure 1), and sediment texture (M-mudstone, W-wackestone, P-packstone, and F-floatstone).

Ichnofabric	Sediment texture	BI	Main ichnotaxa	Secondary ichnotaxa	Tiering
IF1	Floatstone	6	*Thalassinoides*	--	No tiering observed. Completely bioturbated. Mottling texture.
IF2	Wackestone	6	*Thalassinoides*	*Chondrites*	No tiering observed. Completely bioturbated. Mottling texture.
IF3	Packstone to wackestone	5-6	*Thalassinoides*, *Palaeophycus*, *Chondrites*, and *Planolites*.	*Phycosiphon* and *Nereites*.	Upper tier: (1) *Palaeophycus*, (2) *Planolites* and *Nereites*, and (3) *Phycosiphon*. Middle tier: (1) *Thalassinoides* and *Planolites*. Deep tier: (1) *Chondrites*.
IF4	Packstone to wackestone	4-5 (locally 3)	*Thalassinoides*, *Chondrites*, and *Phycosiphon*.	*Palaeophycus*, *Planolites*, *Nereites*, and locally *Zoophycos*.	Upper tier: (1) *Palaeophycus*, (2) *Planolites* and *Nereites*, and (3) *Phycosiphon*. Middle tier: (1) *Thalassinoides* and *Planolites*. Deep tier: (1) *Zoophycos* and (2) *Chondrites*.
IF5	Packstone (locally wackestone)	4	*Thalassinoides*, *Chondrites*, *Planolites*, and *Palaeophycus*.	*Phycosiphon* and locally *Nereites*.	Upper tier: (1) *Palaeophycus*, (2) *Planolites* (and *Nereites*), and (3) *Phycosiphon*. Middle tier: (1) *Thalassinoides* and (2) *Planolites*. Deep tier: (1) *Chondrites*.
IF6	Wackestone	4-5	*Thalassinoides*, *Palaeophycus*, *Planolites*, and *Chondrites*.	*Zoophycos* and *Nereites*.	Upper tier: (1) *Palaeophycus*, (2) *Planolites*, and (3) *Nereites*. Middle tier: (1) *Planolites*, (2) *Thalassinoides*, and (3) *Nereites*. Deep tier: (1) *Zoophycos* and *Chondrites*.
IF7	Wackestone	4-5	*Thalassinoides*, *Chondrites, Palaeophycus*, and *Zoophycos*.	*Phycosiphon* and locally *Nereites*.	Upper tier: (1) *Palaeophycus*, (2) *Phycosiphon* (*Nereites*). Middle tier: (1) *Thalassinoides,* (2) *Phycosiphon* (*Nereites*). Deep tier: (1) *Zoophycos* and (2) *Chondrites*.
IF8	Wackestone	1-2	*Chondrites*, *Thalassinoides* and *Planolites*.	*Phycosiphon*	Upper tier: (1) *Planolites* and (2) *Phycosiphon*. Middle tier: (1) *Planolites* and (2) *Thalassinoides*. Deep tier: (1) *Chondrites*
IF9	Mudstone to wackestone	1-2	*Thalassinoides*, and *Phycosiphon*	*Planolites*.	Upper tier: (1) *Planolites* and (2) *Phycosiphon*. Middle tier: (1) *Planolites* and (2) *Thalassinoides*.

Table 2. Ichnofabrics of IODP Site U1468. The table include the ichnofabric name (IF), sediment texture, bioturbation index (BI, after Hansen and MacEachern, 2007), main and accessory ichnotaxa, and tiering observations. Numbers in the tiering columns indicate the order of colonization at every depth.